On the role of thermal exposure on the stress controlled fatigue behaviour of a high strength titanium–aluminum alloy

Huang, Ze; Sun, C.

DOI:
10.1016/j.msea.2014.07.063

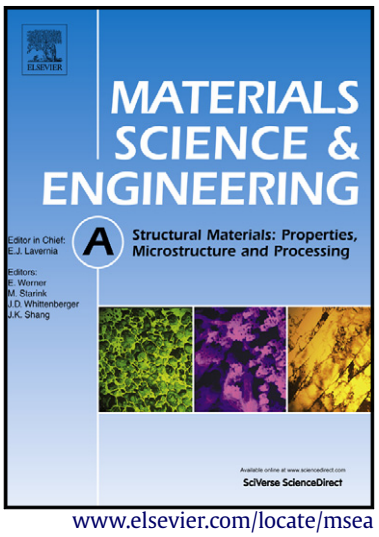

www.elsevier.com/locate/msea

On the role of thermal exposure on the stress Controlled fatigue behavior of a High strength titanium-aluminum alloy

Z.W. Huang, C. Sun

PII: S0921-5093(14)00930-7
DOI: http://dx.doi.org/10.1016/j.msea.2014.07.063
Reference: MSA31382

To appear in: *Materials Science & Engineering A*

Received date: 6 December 2013
Revised date: 17 July 2014
Accepted date: 18 July 2014

Cite this article as: Z.W. Huang, C. Sun, On the role of thermal exposure on the stress Controlled fatigue behavior of a High strength titanium-aluminum alloy, *Materials Science & Engineering A,* http://dx.doi.org/10.1016/j.msea.2014.07.063

On the Role of Thermal Exposure on the Stress Controlled Fatigue Behavior of a High Strength Titanium-Aluminum Alloy

Z.W. Huang[a,b*] and C. Sun[a]

[a] School of Materials Science and Engineering, Southwest Jiaotong University, Chengdu, Sichuan, 610031, P.R. China

[b] Department of Metallurgy and Materials, The University of Birmingham, Edgbaston, Birmingham B15 2TT, U.K.

∗Corresponding author, Tel: 44 121 414 3436
Email address: zewenhuang9@sohu.com

Abstract

Fatigue specimens with four types of surface were assessed under three exposure conditions (no exposure, block exposure, individual exposure-oxidation at 700°C for 10000 h) to quantify the effects of surface roughness, stress concentration, oxidation and inner microstructural embrittlement on fatigue strength of a near lamellar γ-TiAl alloy Ti-44Al-4Nb-4Zr-0.2Si-1B. With the yield strength of $\sigma_{0.1}$=621MPa, S-N fatigue is found to be always conducted under a loading condition of $\sigma_{max}<\sigma_{0.1}$. Local plastic deformation is difficult to occur on the maximum-stressed surface. The surface quality with or without defects and residual stresses therefore becomes critical for fatigue performance. Introducing compressive-stressed layer by shot peening and removing tensile-stressed layer and defects by grinding-electropolishing can improve the fatigue strength significantly, and the latter is more capable than the former for the high strength alloy. It is found that the fatigue performances of all types of surface are deteriorated to some degree when subjected to block exposure, owing to exposure-induced embrrittlement. On the other hand, exposure-induced fatigue strengthening occurs after individual exposure-oxidation. The relaxation of residual tensile stress and dissipation of bulk stress in warm-air environment are found to outweigh the negative effects of oxidation layer at surface and exposure-induced embrittlement inside specimen.

Keywords: Gamma titanium aluminides; Thermodynamic stability; High cycle fatigue; Surface damage; Notch sensitivity; Scanning electron microscopy

1. Introduction

γ-TiAl based intermetallic alloys exhibit much steeper fatigue crack growth resistance curves and lower fracture toughness than conventional Ti-based and Ni-based alloys. Such characteristic features give rise to a relatively narrow interval between the threshold stress intensity factor range ΔK_{th} and the maximum stress intensity factor K_{max} at final failure [1-5]. The fraction of total fatigue life resulting from crack propagation is therefore significantly small, and the total life is likely to be dominated by the number of cycles to crack initiation. Based on this behavior, one approach to a reliable prediction of fatigue life for γ-TiAl alloys is to use conventional S-N fatigue curves. Fatigue strength, as a representative of fatigue crack initiation resistance, is considered to be one of the primary design drivers for TiAl alloys [6-8].

In view of the importance of endurance limit based on S-N performance, there is a need to develop a clear understanding of how surface defects and other stress concentrators, caused by component design, manufacturing and machining, impact of foreign object and surface oxidation, affect the total life of γ–TiAl alloys under cyclic loading. The degree and extent to which fatigue strength is reduced by surface defects and stress concentrators should be assessed quantitatively. This becomes particularly important since γ-TiAl alloys often exhibit a relatively flat fatigue S-N curves [9-11]. Any stress raisers in components, even on a small scale, could cause over-stressing and thus unexpected early failure. Considerable amounts of research have been carried out to qualify the effects of surface quality [12-15], notch [16, 17], foreign object damage [18, 19] and oxidation layers [20, 21] on fatigue life of TiAl alloys. However, no much effort in this area has been made for γ-TiAl alloys which are subjected to a long-term thermal exposure. A γ-TiAl based alloy component in service is in fact exposed

to elevated temperatures (say 700°C) in air environment for long time (say 10000 hours). Three major types of microstrcural/micromechanical changes are expected to occur: a) internal microstructual changes due to constituent dissolution, decomposition and phase transformation, b) surface layer oxidation and c) changes in suface and bulk stress concentration since long-term exposure in a thermal enviroment. Therefore, it is necessary to assess all the surface defects and stress concentrations on total life under the condition of long-term thermal exposure in air.

The present study concentrates on all these effects on the total life of a high-strength, fine-grained γ-TiAl alloy. The alloy is to be studied under three thermal exposure schemes: a) no exposure, b) block exposure with internal changes but no surface oxidation, c) thermal exposure with both internal changes and surface oxidation. The main objective of the study is to reveal how and to what extent the varied surface and bulk material under the three thermal exposure schemes affect the fatigue crack initiation resistence of the high strength TiAl alloy. This work concerning damage tolerance capability in real service is expected to provide a reference guide for safe applications of TiAl alloys at elevated temperatures.

2. **Experimental**

The γ-TiAl based alloy in this study is a grain refined, high strength ($\sigma_{0.1}$= 621 MPa) near lamellar alloy Ti-44Al-4Nb-4Zr-0.2Si-1B (alloy 4Nb-4Zr). The alloy ingot was produced using a double-melted PACH (Plasma Arc Cold Hearth) process. The ingot received was approximately 100 mm in diameter, and was hot isostatically pressed (HIPped) at 1260°C under a pressure of 150 MPa for 4 hours. The alloy composition was determined by inductively coupled plasma atomic emission spectrometry (ICP-AES) for the main elements, and is Ti-43.73Al-4.14Nb-4.12Zr-0.24Si-1.01B (at. %).

Three groups of specimens with different thermal exposure history were prepared for

S-N fatigue testing: Group A, no exposure; Group B, exposure in ingot block without oxidation; Group C, individual specimen exposure with surface oxidation. Fatigue specimens of dimensions 10 x 10 x 70 mm^3 were machined from as-HIPped ingot. Four surface conditions were prepared for each group: plane-sided EDM wire, V-notch, shot-peened and electropolished. The details of the preparation procedures were listed in Table 1. A 60° V-shaped notch (V-notch) with a root radius of 0.20 mm and overall notch depth of 1.75 mm ($K_t = 3$, where K_t is the theoretical elastic stress concentration factor) was introduced. Notch was machined using one pass EDM wire, same as plane-sided EDM specimens. Shot peening was carried out by means of an injector type system using ϕ 0.4-0.5 mm sized zirconia-based ceramic spheres at an air-jet pressure of 5×10^5 Pa. The peening was done to achieve a full coverage of the maximum-stressed surface area. Electropolishing was carried out on mechanically ground and polished samples and performed at 20 volts in an electrolytic solution of 6% perchloric acid, 35% butanol and 59% methanol at - 25°C.

Table 1 The preparation procedure of the maximum stressed surface for fatigue tests

Surface	Preparation procedure
EDM wire	One pass EDM wire to shape
V notch (Kt = 3)	One pass EDM wire to shape
Shot peening	One pass EDM to shape, grinding, shot peening
Electropolishing	One pass EDM to shape, grinding and polishing, electropolishing

Surface roughness was measured using an Ambios XP-2 profilometer over a distance of 5 mm and represented in a standard Ra value. The Ra value listed in Table 2 is an average of 5 measurements for each surface condition, with an error range assessed by standard deviation. The surface roughness was measured before individual exposure-oxidation for Group C, which was measured in the same batch with non-exposed Group A. Therefore, samples in Group C and A display the same surface roughness. However, due to 10000-h exposure before shape machining and surface preparation, the surface roughness of Group B specimens shows values slightly different from those in Group A and C.

Microhardness profiles were measured to characterise the compressively strained surface after shot peening. The measurements were conducted on a HXD-1000TM Vickers micohardness tester with a load of 100 g.

Table 2 Surface roughness Ra (μm) with error range for each surface condition

Specimen (Group)	EDM (A, C)	Shot peening (A, C)	Electropolishing (A, C)	EDM (B)	Shot peening (B)	Electropolishing (B)
Surface roughness Ra (μm)	4.60±0.13	1.51±0.20	0.31±0.03	5.22±0.10	1.55±0.11	0.32±0.04

After surface preparation, specimens in Group A were fatigue tested directly (named "no exposure"), while those in Group C were exposed individually in an air-circulated furnace at 700°C for 10000 h (named "individual exposure-oxidation"), and then tested after exposure. In contrast to Group C, Group B was exposed as a 100 mm diameter ingot block (named "block exposure") in the same furnace at 700°C for 10000 h, and then machined to shape and prepared for the same four surface conditions, followed by fatigue testing. It appears that all specimens in Group B experience interior microstructural changes but no oxidation at the surface.

S-N fatigue tests were carried out at room temperature in ambient air. Four point bending samples were tested on a PLG-100 electromagnetic resonance testing machine at a frequency of 100-120 Hz under a stress ratio R of 0.1 (where $R = \sigma_{min}/\sigma_{max}$, and σ_{min} and σ_{max} are the minimum and maximum stresses applied over the fatigue cycle respectively). Testpiece run-out was defined for specimens not failing after 10^7 cycles. The fatigue limit σ_{FL} is typically defined by the value of σ_{max} at run-out ($\geq 10^7$ cycles).

The prepared surfaces and microstructures before and after thermal exposure were examined by scanning electron microscopy (SEM) utilising either secondary electron (SE) or backscattered electron (BSE) mode. The average colony/grain size, obtained from more than 1000 colonies/grains, was determined using linear interception method. The volume fraction of α_2 and γ phases was measured using Image J software on several BSE images. Detailed

microstructure before and after thermal exposure were also studied by transmission electron microscopy (TEM) using a JEOL 2010 FX microscope operating at 200 kV. Thin foils were prepared by twin-jet polishing with an electrolyte of 5 vol. % perchloric acid, 30 vol. % butan-1-ol and 65 vol. % methanol, operating at 30 V and at a temperature of -30°C. For all image analyses, mean values were determined with a standard deviation to represent the uncertainty of the measurements.

3. **Results**

3.1. The microstructure before exposure

The microstructure of the alloy 4Nb-4Zr before exposure is shown in Fig. 1a**.** The alloy after HIPping essentially shows a near-lamellar (NL) microstructure, consisting of lamellar colonies (70 ± 11 μm in size and ~70 vol. %) and equiaxed β, α_2 and γ grains (5-20 μm in size and ~ 30 vol. % in total). The β (B2 structure with ω precipitation), accounting for 9 vol. % after 1260°C HIPping, is the remnant of uncompleted phase transformation $\beta \rightarrow \alpha$ during ingot cooling. The formation of β (B2+ω) is attributed to addition of 4Nb and 4Zr: the former serves as a β stabilizer while the latter a ω stabilizer [22, 23]. The retained β in the alloy exhibits a cellular morphology, consisting of numerous micron-sized cells. The majority of the cells show smooth surface, while some, especially those near the cell interfaces, look rough (Fig. 1c).

3.2. The microstructure after exposure

The material in Group B was exposed as a 100 mm diameter ingot block for 10000 h at 700°C before machined to shape and surface preparation. No oxidation layer formed on the surface except for the changes in bulk material. In contrast to Group B, the material in Group C was exposed as individual samples (10x10x70 mm^3). Both oxidation and changes in bulk

material occurred on the Group C samples.

The changes in bulk material induced by 10000 h-exposure were characterized in detail in a previous paper [24]. A brief description is given here. The changes mainly occurred in prior β (i.e. B2+ω) grains, consisting of three types of phase transformation/precipitation. The first was the formation of block-shaped γ grains. The transformation of γ from β showed black spot images under BSE microscopy (Fig. 1b) and irregular blocks in bright field TEM (Fig. 1d). The phase transformations β (B2+ω) → γ after long-term exposure at 700°C was thought to be an equilibrium-returning process, aiming to decrease the excess β. This was similar to α_2 → γ which occurred during exposure if α_2 volume fraction was stoichiometrically far from equilibrium. The second change in the prior β regions was characterized by extensive precipitation of fine $D8_8$-ω particles from $B8_2$-ω cell matrix. As arrowed in Fig. 1d, nanometer sized $D8_8$-ω particles precipitated significantly from the cell matrix, which was clear and clean before exposure (Fig. 1c). The lattice structures of both $D8_8$-ω and $B8_2$-ω were confirmed by a serial analysis of diffraction patterns in previous studies [23, 24]. The third was the precipitation and growth of $(Ti,Nb,Zr)_5(Si,Al)_3$ silicides at cell interfaces (Fig. 1d) and grain boundaries (not shown). This phenomenon can be seen clearly by comparison between Fig. 1d and Fig. 1c. These silicides were near-spherical in shape and ~ 100 nm in size after 10000 h exposure.

All the three types of phase transformation/precipitation were considered to be detrimental to alloy 4Nb-4Zr owing to decreasing the ductility significantly. This phenomenon was called "exposure-induced embrittlement" in the previous research [24].

3.3. The fatigue-specimen surfaces prepared before exposure

As shown in Fig. 2a, one-pass EDM wire produced a damaged surface layer containing widespread holes (tens of micrometer in size), protruded globes and fine cracks (arrowed)

due to local melting and erosion induced. The Ra values representing the one-pass EDM surface roughness are high, as given in Table 2. Fig. 2b reveals that the surface cracks caused by EDM wiring can run down to ~40 μm below the loose surface. Previous work found that a high level of tensile residual stress (~300 MPa) was induced at near-surface position after one-pass EDM wire of a low strength γ–TiAl based alloy [9]. The tensile stress level could be even higher in high strength alloy [14] such as the alloy 4Nb-4Zr since less degree of plastic deformation would be expected. Such a high level of tensile stress at the EDM surface is thought to be responsible for the widespread surface cracking.

EDM surface was ground before shot peening. Shot peening of the ground EDM surface actually produced a relatively integrated surface with a number of shallow dimples and puckers, see Figs. 3a and 3b. The Ra value after shot peening was reduced to 1/3 of the EDM value (Table 2). Cross-sectional view of the peened specimen reveals a deformed region underneath the peened surface (Fig. 3b), which is characterized by considerable bending of the lamellae. The deformed region is ~10 μm in depth. Small holes were observed in the near surface region. They were produced very possibly by coming off of broken B2+ω cells (indicated by wide arrow) and TiB_2 particles (by fine arrow). Both are hard and brittle in nurture and prone to cracking under strong mechanical impact force. However, a survey of the shot peened surface shows that the bending of the lamellar structure is not uniform across the peened surface. The lamellae are barely deformed if they are perpendicular to the peened surface, see Fig. 3c. This suggests a hard orientation, along which the angle ϕ between the lamellae interfaces and shot stream is zero [25]. It is observed in Fig. 3c and the insert that some of α_2 lamellae break up into short sections under the bombarding force of ceramic particles while mechanical twining occurred in γ lamellae. This phenomenon is attributed to the harder and more brittle nature of α_2 lamellae than γ lamellae. It is well documented that the α_2 phase in $\alpha_2+\gamma$ two-phase alloys scavenges interstitial impurities such as oxygen, nitrogen and carbon [26-29], which leads to a significant solution

hardening and thus makes deformation more difficult in α_2 than in γ lamellae.

Shot peeing also caused a significant conversion of the microstructure in the near surface layer. Dynamic recrystallization (DR) and phase transformation occurred both inside lamellar colonies (Fig. 3c) and inside equiaxed γ grains (Fig, 3d). As indicated by DR and arrows in Fig. 3c, very fine γ grains were nucleated and grown through dissolution of α_2 and γ lamellae, indicating that the $\alpha_2 \rightarrow \gamma$ phase transformation occurred locally. The morphology of the recrystallized γ grains in the equiaxed γ grains became less clear (arrowed in Fig. 3d), suggesting that the formation of high angle boundaries may not complete. The stress-induced dynamic recrystallization and phase transformation seems more active in lamellar colonies than in equiaxed γ grains. This is understandable since higher stress condition is expected in $\alpha_2+\gamma$ two phase region than in single γ region under shot peening.

As a result of the process-induced deformation and compressive stress, the microhardness in the near-surface regions significantly increased, and a maximum value obtained at the surface, as shown in Fig. 4. It can be seen that both the specimens without exposure (Group A) and the specimens with block exposure (Group B) show a ~ 260 μm-thick hardened region with a microhardness value at the surface ~ 200 HV0.1 higher than the bulk values, indicating that the hardening at the surface is about 50 % for the two groups. The similarity in compressive stressed and hardened layer for Group A and B is understandable since the samples in Group B were EDM machined to shape after block exposure, and then subjected to shot peening. In contrast to Group A and B, Group C samples were shot peened before individual exposure. It is seen from Fig. 4 that the individually exposed-oxidized samples in Group C demonstrate a reduced near-surface hardening region after individual exposure to 700°C warm air for 10000 h. Compared with the bulk value, the hardness increase at surface is reduced from 50% to 30% and, the thickness of the hardened region reduced to 140 μm, roughly halved the depth of the original processed region due to exposure and oxidation.

Fig. 5a shows the elecropolished surface before exposure. The major constituents of the alloy can be observed under the BSE mode. The Ra value after elecropolishing was reduced to only 1/5 of the shot-peened value. The grinding and polishing plus electropolishing procedure used in this study is found to be able to take off a ~150-200 μm thick surface layer, which is deep enough to remove the whole EDM-damaged surface layer and even a thin layer underneath it. The surface defects were removed sufficiently as a result, leaving an almost defect free surface prior to fatigue testing. Fig. 5b, a SE image, reveals that such a surface finish on the maximum-stress side is smooth and nearly defect-free after electropolishing.

It should be mentioned here that the EDM wired, shot peened and V-notched surfaces prepared in Group B are very similar in morphology to those in Group A, respectively. Therefore the three types of surface in Group B are not shown here. However, the microstructural changes due to block exposure can be observed on the electropolished surface in Group B. The precipitation of γ grains, $D8_8$-ω particles and $(Ti,Nb,Zr)_5(Si,Al)_3$ silicides from the β matrix can be easily observed in the mirror-like surface under BSE mode. The image is not shown here but should be no difference from those shown in Fig. 1b.

3.4. The fatigue-specimen surfaces after exposure and oxidation

Group C specimens were exposed individually at 700°C for 10000 h in air. Both interior changes in bulk material and surface oxidation occurred. The normal and cross-sectional view of the oxidised EDM specimen is shown in Fig. 6a and 6b, respectively. It can be seen that the numerous holes, globes and cracks formed on EDM surface are now covered by an oxidized scale, and the surface looks still rough (Fig. 6a). The oxidation scale is about 25 μm thick (Fig. 6b). Fig. 6c, a BSE image at a larger magnification, shows that a solid layer of equiaxed γ grains formed underneath the oxidation layer, followed by lamellar colonies towards bulk material. It is noted that the prior β grains, which accounts for 9 vol. % in bulk material (Fig. 1), cannot be observed in the subsurface region until ~ 300 μm inside. It is well

documented that during oxidation, heavy metals like Nb and Zr which partitioned originally in β(B2+ω) grains would diffuse towards surface to form Zr- and Nb-containing oxides [30-33]. These oxides normally reside with TiO_2-Al_2O_3 oxidised layers. Some clusters with brighter contrast are observed in the oxidation layer of the EDM surface, as indicated by coarse arrows in Fig. 6c. They might be the Nb and Zr containing oxides. Therefore, it is the diffusion of Nb and Zr towards the surface that causes the disappearance of β(B2+ω) grains. It is somewhat surprising to find a layer of equiaxed γ grains below the oxidation scale. The formation of γ grains indicates that an Al-rich sub-surface rather than an Al-depleted zone was formed during oxidation. The enrichment of Al in the subsurface region has been widely reported by previous research [34-37], but not necessarily formed as a γ grain layer. It is tempting to speculate that the formation of the γ grain layer is caused by active diffusion of Ti, Nb, Zr towards the scale, and thus leading to α_2-dissolution during oxide/nitride formation.

The oxidised scale of shot peened specimen looks relatively flat and less cracking, compared with that of EDM specimen. Shallow dimples are still observable on the oxidised surface, see Fig. 7a. Cross sectional view of surface has found that the oxidized scale is narrower than its EDM counterpart , about 15 μm in thickness (Fig. 7b). In contrast to EDM surface, no γ grain and lamellar layers form beneath the oxidized scale. Correspondingly, the β grains do not disappear in the subsurface region, but become less solid (indicated by letter A in Fig. 7c). A high density of white particles is observed to distribute inside lamellae and γ grains across ~ 30 mm distance from the surface. Fig. 7c, a BSE image at a higher magnification, shows that these particles are normally needle-shaped and distribute in geometric patterns. The nature of the widespread particles could not be identified. They might be the Nb/Zr/Ti-containing oxides (bright under BSE) that formed along deformed traces in the heavily deformed subsurface region.

The elecropolished surface is covered by loose scale after 10000 h exposure-oxidation at 700°C in air. The scale still retains the lamellar and equiaxed γ morphology of the alloy (Fig.

8a). This was explained duo to the different oxides formed above the γ-TiAl lamellae and α_2-Ti_3Al lamellae. The oxides covering γ-TiAl lamellae consisted of an Al-rich oxide, likely Al_2O_3; while the oxides covering α_2-Ti_3Al lamellae consisted of an Al-rich oxide covered by a very porous and discontinuous Ti-rich oxide, probably rutile TiO_2 [36]. Cross sectional observation of the oxidised surface and subsurface in Fig. 8b has found that the scale is about 10 μm thick after 10000 h at 700°C, which is the narrowest among the three types of surface. The oxidized subsurface shows microstructural features similar to the shot peened: no γ grain and lamellar layers form beneath the oxidized scale, but also no β grains disappear in the subsurface region. Again, a high density of white particles is observed to distribute inside lamellae and γ grains, across ~ 50 mm distance from the surface. Fig. 8c, a BSE image at a higher magnification, shows that these particles are normally needle-shaped and distribute in geometric patterns. They may even connect to each other to become linear-shaped. The nature of the particles could not be identified. Once again, they might be the Nb/Zr/Ti-containing oxides that form on the dense-packed planes. More work is needed to clarify and characterize these bright particles.

3.5. The stress-fatigue behavior of Group A specimens

For EDM specimens with severe surface damage, no matter what exposure history have experienced, a "go-no go" S-N data pattern was generally observed: specimens either failed at low number of cycles or run out without failure, seldom broke in between. This means that a small increase in applied stress (e.g. 5-10 MPa), or even no increase in stress, the number of cycles to failure can drop from run-out ($\geq 10^7$ cycles) to less than 10^5 cycles. The worst situation is that the specimen may run out at a higher peak stress but failed earlier at a lower peak stress, as indicated by a pair of arrows in Fig. 9a and 9b. Such flat S-N curves and the related uncertainties were reported previously by several researchers [9-11, 38].

Fatigue strength data are listed and analysed in Table 3 for the three types of plane-sited

surface which were exposed in three groups. All the percentage data in Table 3 are approximated to the nearest integer. As seen in Table 3, the σ_{FL} at run out (280 MPa) for the EDM wired surface before exposure is much lower than 0.1 proof stress ($\sigma_{0.1}$=621MPa). The $\sigma_{FL}/\sigma_{0.1}$ ratio is only 0.45 and σ_{FL}/σ_{UTS} is only 0.42 (σ_{UTS} = 665MPa) for the high strength alloy 4Nb-4Zr, which is significantly lower than those obtained in a wide spectrum of TiAl alloys [8-10]. The severe deteriorated fatigue resistance under EDM condition is usually attributed to EDM surface which is covered by widespread defects and contains a high level of tensile residual stress. But previous studies found that the degree of the loss in σ_{FL} caused by EDM was related to the alloy strength. The fatigue limit of EDM surface could be still greater than its yield strength in a low strength ($\sigma_{0.1}$ = 310 MPa) TiAl alloy [9], and remarkably less reduced in an intermediate strength (σ_y =486 MPa) TiAl alloy [39]. It seems to suggest here that the fatigue behaviour of the high strength alloy is highly sensitive to the harmful surface.

Table 3 S-N fatigue results and data analysis for EDM, shot peening and electropolishing specimens ($\sigma_{0.1}$=621MPa before exposure, $\sigma_{0.1}$=641 MPa after exposure)

Exposure Condition (Group)	Specimen surface Condition	σ_{FL} (MPa)	$\sigma_{FL}/\sigma_{0.1}$	Increase in σ_{FL} (%) relative to EDM	Change in σ_{FL} (%) relative to Group A
No exposure (Group A)	EDM wire	280	0.45	—	—
	Shot peening	380	0.61		
	Electronpolishing	470	0.76	36	
Block exposure (Group B)	EDM wire	240	0.37	—	-14
	Shot peening	350	0.55		-8
	Electronpolishing	340	0.53	46	-28
Individual exposure -oxidation (Group C)	EDM wire	450	0.70	—	61
	Shot peening	475	0.74		25
	Electronpolishing	530	0.83	6	13

Table 3 also reveals that the high strength alloy 4Nb-4Zr is sensitive to surface improvement concerning the σ_{FL} increment. For example, shot peening of the EDM surface improves fatigue strength remarkably, increased by 36% in non-exposure condition. This result is consistent with the hardened and more integrated layers formed by shot peening, as described in section 3.3. In fact, shot peening not only removed the electricity-eroded EDM

surface but also produced a compressively stressed layer with significant hardening in the outer 260 μm of the specimens, even though surface cracks were not totally removed.

Moreover, electropolishing after mechanical grinding and polishing has produced a nearly "defect-free" surface. Consequently, electropolishing of the EDM surface is able to increase fatigue strength by 68% before exposure. It appears that the defect-free surface outperforms the shot peened surface despite there is no compressively-stressed outer layer at the electropolished surface. There are contradictory results concerning the relationship of shot peening and electropolishing in literature. In contrast to the present result, the research conducted by Lindemann, et al. showed that shot peened samples had fatigue strength 125-300 MPa above their electropolished reference samples [15]. However, the results from Wu, et al. showed that the electropolishing can outperform the shot peening in a high strength TiAl alloy ($\sigma_{0.2}$ = 625 MPa) [14]. It is assumed that the different outcome could be due to the specific procedures and parameters used.

S-N data for the V notch (Kt=3) fatigue tests are presented using net section in Table 4. As would be expected, the fatigue limit σ_{FL} reduced significantly for V notched specimens: from 280MPa in plane-sided specimens to 100MPa. A fatigue notch factor K_f = 2.8 and a ratio of K_f/K_t = 0.93 is obtained for non-exposed condition. K_f is the notch factor used to express the effectiveness of the notch in decreasing $\sigma_{FL,}$ while K_t is the theoretical elastic stress concentration factor in the present case. Here, K_f is calculated based on σ_p/σ_n (σ_p and σ_n are the fatigue limit for plane-sided and notched specimens, respectively). It is generally recognised that if fatigue notch factor K_f is close to the value of K_t, the material is regarded as sensitive to notch. In the present work, the ratio of K_f/K_t = 0.93 in Group A is not very far from the extreme value K_f/K_t = 1, indicating a high notch sensitivity for the non-exposed alloy 4Nb-4Zr. The notch sensitivity can also be represented by notch sensitivity factor Q (Q = K_f-1/K_t-1). As seen in Table 4, Q is 0.9 for Group A, which is also close to the extreme value 1.

Table 4 S-N fatigue results and data analysis for V notch (K_t=3) specimens ($\sigma_{0.1}$=621MPa)

Exposure condition (Group)	σ_{FL} (MPa)	$\sigma_{FL}/\sigma_{0.1}$	K_f	K_f/K_t	Notch sensitivity factor Q
No exposure (Group A)	100	0.16	2.80	0.93	0.90
Block exposure (Group B)	120	0.19	2.00	0.67	0.50
Individual exposure-oxidation (Group C)	170	0.27	2.65	0.88	0.83

3.6. The stress-fatigue behavior of Group B specimens

On comparison of EDM wired, shot peened, and electropolished specimens in Group B with their counterparts in Group A, it is found from Table 3 that every type of the surface has the fatigue strength inferior to its counterpart in Group A. A noticeable decrease (-14%) is obtained for the EDM surfaces, a marginal decrease (-8%) for the shot peened and a considerable decrease (-28%) for the electropolished. All the results indicate that block exposure at 700°C for 10000 h is detrimental to fatigue performance for every surface.

Decrease of the fatigue strength from 280 MPa to 240 MPa brings the $\sigma_{FL}/\sigma_{0.1}$ ratio further down to 0.37 ($\sigma_{0.1}$ = 641 MPa) for the EDM surface after block exposure. This value is uniquely low in γ-TiAl based alloy family. Although the EDM surface of Group B looks very similar to their Group A counterpart, the alloy after block exposure becomes more vulnerable to crack initiation. The deteriorated fatigue behaviour is deduced to come from "exposure-induced embrittlement", which occurred in bulk material during long-term exposure. As mentioned before, the embrittlement was caused by a series of profound microstructural changes, mainly the precipitation of γ grains, $D8_8$-ω particles and $(Ti,Nb,Zr)_5(Si,Al)_3$ silicides from the β matrix. They are relatively brittle in nature than the parent phase. These brittle phase/particles may provide more crack nucleation/initiation sites, especially when located along cell/grain boundaries. Therefore, these changes exacerbate the already damaged EDM surface and make the EDM surface more susceptible to crack

nucleation and initiation.

The decrease in fatigue strength is also observed in shot peened and electropolished specimens after block exposure: 8% decrease with the deformed and hardened surface layer but 28% decrease with a "defect-free" surface at which no surface deforming and hardening occurred. As a consequence of the greater decrease, the better-performed electropolished surface before exposure becomes slightly inferior to shot peened surface after block exposure. The shot peened surface can limit the negative influence from block exposure more effectively than the electropolished does, probably because hardening a surface layer could force initiation sites to shift to subsurface region at a depth which corresponds to the size of the compressive zone. For electropolished surface which is less resistant to the detrimental effect from block exposure, it tends to suggest that with the reduced impact from surface defects, the fatigue behavior could be increasingly governed by inner microstructure. Therefore, interior embrittlement could have a great role to play.

The notch sensitivity is found to reduce significantly after long-term exposure. The value of Q is only 0.5 after block exposure. The significant decrease in K_f, Q value and K_f/K_t ratio for V notch specimens in Group B seems inconsistent with the exposure-induced embrittlement phenomenon. No stress relaxation near the notch root was expected since all the specimens were machined to shape after block exposure. The reason behind these reductions remains unknown. The much reduced notch sensitivity may be an outcome of significantly reduced σ_{FL} in EDM plane-sided specimens (240MPa) or may come from experiment error since the degree of uncertainty for the brittle alloy in high cycle S-N fatigue testing is high.

3.7.The stress-fatigue behavior of Group C specimens

Respective comparison of the EDM wired, shot peened and electropolished fatigue performance between Group C and Group A shows that every type of the surface in Group C has the fatigue performance superior to its counterpart in Group A. A significant increase (61%) in σ_{FL} is obtained for the EDM surfaces, a much reduced but still considerable increase (25%) for the shot peened but a marginal increase (13%) for the electropolished. The superior fatigue performance is even obtained in V-notched specimen. As seen in Table 4, the fatigue limit σ_{FL} is increased from 100 MPa before exposure to 170MPa after individual exposure-oxidation, indicating a 70% increase. All the results indicate undoubtedly that individual exposure-oxidation at 700°C for 10000 h can improve fatigue performance for the four types of surface. The enhanced S-N fatigue performance seems unexpected since oxidation scale was formed and interior embrittlement was induced after 10000 h individual exposure-oxidation treatment.

It is interesting to find that the degree of the fatigue strengthening achieved in Group C over Group A is reversely related to the quality of the surface prepared. For the three plane-sited specimens, the highest increase (61%) is obtained for the worst surface (EDM surface); the increase in σ_{FL} reduces to 25% for the shot peened and further down to 13% for the electropolished. The test results indicate that the worst EDM surface which contains highest tensile stress and most widespread defects has the greatest potential for fatigue resistance improvement through individual exposure and, the potential is reduced with improving surface quality. It can be seen that after such a long-term individual exposure, the three types of plane-sided surface in Group C end up having increasingly similar fatigue behaviour than in other two groups. This phenomenon appears to be related to the warm environment and the prolonged duration of exposure time.

Corresponding to the increased similarity in fatigue performance, the surface improvement procedures used in this study become less effective in raising fatigue resistance after individual exposure-oxidation. As shown in Table 3, the positive contribution of shot peening to fatigue strength over EDM reduces from 36% in Group A to only 6 % in Group C. For the electropolished surface, the improvement of fatigue strength reduces from 68% in Group A to 18 % in Group C. The significantly declined achievement in shot peened surface is considered to be related to thermal relaxation of compressive stresses in the outer layer. As shown in Fig. 4, the thickness of the hardened layer was halved and the hardness value was reduced markedly. The declined in electropolished surface should be attributed mainly to the formation of oxidation layer.

Corresponding to the increase in fatigue strength by 70%, the notch sensitivity factor Q ($Q = K_f\text{-}1/K_t\text{-}1$) reduced after long-term exposure-oxidation, from 0.9 before exposure to 0.83 after individual exposure-oxidation. Long term exposure-oxidation of individual specimens is expected to dissipate the stress concentration near the notch root to some degree, therefore decreasing the notch sensitivity.

Discussion

4.1. Surface-quality control mechanism

With the yield strength of $\sigma_{0.1}$=621MPa (641MPa after exposure), fatigue testing was always conducted under a loading condition of $\sigma_{max} < \sigma_{0.1}$ for the high strength alloy 4Nb-4Zr. Under this condition, plastic deformation through intense planar slipping and twining is unlikely to be activated in the surface layer where maximum stress is applied. The derivative microcracks are therefore relatively difficult to nucleate through the deformation mechanisms. Fractographic examination on the fracture surface of an electropolished sample (σ_{max} = 600 MPa with N_f=2300 cycles) has found no noticeable plastic deformation in the near surface region which is most highly stressed under cyclic loading (Fig. 11). Plastic deformation

inside lamellar colonies was normally characterised either by geometrically arranged parallel steps or by delaminated big facets [40, 41]. Without intense deformation in the surface-subsurface layers, the surface quality with or without defects and/or residual stresses becomes increasingly important for fatigue behaviour. Any defects at the surface may act as stress raisers to cause some degree of stress concentration, which could force testpieces into a loading condition of $\sigma_{max} > \sigma_{0.1}$ locally, thereby resulting in localised plastic deformation and crack nucleation, and leading to crack initiation and fast propagation. On the other hand, removing harmful residual stresses and defects would certainly improve fatigue crack nucleation/initiation resistance since loading peak stresses are lower than yield stress.

Pre-yielding initiation is easy to take place on EDM-wired specimens since a damaged surface with high tensile stress and widespread defects was produced. It was found by S. J. Trail and P. Bowen that high residual tensile stresses were introduced to the surface-subsurface layer by EDM [9]. The stresses presumably arose from localised melting, rapid solidification and thermal contraction owing to strong electric current involved. When superimposed on the applied fatigue stresses, the residual tensile stresses are expected to effectively increase the mean stress of the fatigue cycle and decrease the fatigue life for crack initiation. Under the worst condition, no crack nucleation stage is needed. Instead, EDM specimens may directly enter a crack initiation stage if the maximum stress on the surface layer is higher than the threshold value for crack initiation.

Based on the “surface-quality control” mechanism, shot peening, as an effective surface-quality improvement technique, is sure to increase the fatigue perofrmance for alloy 4Nb-4Zr. As shown in Figs. 2 and 3, shot peening of the EDM surface has removed the EDM damaged surface layer and tensile residual stresses. More importantly, the process has produced a hardened and increasingly integrated layer, where plastic-elastic deformation and compressive stresses were introduced into the outer 260 μm of the specimen. Hardening a surface layer could force initiation sites to shift to subsurface region at a depth which

corresponds to the size of the compressive zone. As a result, fatigue limit at run-out increased by 36% before exposure.

Compared with shot peening, electropolishing is found to be more capable of improving crack initiation resistance for the high strength alloy 4Nb-4Zr: 68% increase in electropolishing over EDM, while only 36% increase in shot peening over EDM. This is because mechanical grinding-polishing of EDM surface, as the first step, has removed a 150-200 μm thick surface layer which is thick enough to remove all surface defects effectively and reduced tensile residual stress tremendously. The following electropolishing process has produced an almost defect-free surface. For fatigue under the loading condition of $\sigma_{max} < \sigma_{0.1}$, such a defect-free surface plays a very important role in increasing fatigue life since a crack nucleation phase is needed and the number of cycles for a nucleated microcrack to become initiated could be large.

Introduction of a V-notch has caused stress concentration to occur and the highest levels should be found at the notch root. Therefore, the notched specimens in this study show reduced fatigue limit, and almost to the extent that the theoretical K_t value of the V-type notch would have predicted. This indicates that the alloy 4Nb-4Zr is sensitive to notch since the fatigue notch factor K_f (K_f = 2.8) is quite close to the value of K_t (K_t =3), and the notch sensitivity factor Q (Q = 0.9) is close to the unit value 1. The high notch sensitivity of alloy 4Nb-4Zr might be related to the fact that the most of the V notched specimens were tested under loading condition of $\sigma_{max} < \sigma_{0.1}$ (here K_t should be taken into account when determining the σ_{max} at notch root). No considerable deformation at notch root is expected, and thus no considerable “notch strengthening” can be obtained. The notch strengthening effect was observed in other TiAl alloys which showed a relatively low yield stress [9, 39].

4.2. Effect of block exposure

There is a good reason to believe that the effect on fatigue performance of Group B comes entirely from the microstructural changes of bulk material. Such changes, including the formation of γ grains, $D8_8$-ω particles and silicides in the β matrix, should be found both on the surface and inside the specimen. This is determined by the way the material was exposed and the way the surface is prepared. As mentioned in section 2, all material in Group B was exposed as a Φ 100 mm ingot block, then machined to shape, and followed by surface preparation. Under this procedure, the microstructural changes due to block exposure can remain on the EDM wired, shot peened and V-notched surfaces, but cannot be observed owing to the damaged and deformed surface finish.

S-N fatigue is also conducted under the loading condition of $\sigma_{max} < \sigma_{0.1}$ for all the block-exposed specimens. Therefore, the fatigue crack nucleation/initiation in Group B always occurred prior to yielding. Under this loading condition, the surface quality again is very important in determining the fatigue performance. As mentioned before, the block exposure has caused a series of changes in bulk material. The transformed phase and precipitated particles are relatively brittle in nature. They could serve as crack nucleation and initiation sites, especially when located at cell/grain boundaries. It seems reasonable to infer that such changes could exacerbate the already damaged EDM surface by providing more favoured sites for microcrack nucleation/initiation, therefore causing a noticeable decrease (14%) in fatigue performance.

A marginal decrease in fatigue strength (8%) is obtained in shot peened specimens in Group B over Group A. Considering the uncertainty related to the S-N data of TiAl alloys, it could claim that the shot peened surfaces both before and after exposure provide a similar fatigue performance. This is true since the deformed-hardened surfaces are quite similar to

each other, as revealed in Fig. 4. It tends to suggest that the deformed-hardened surface layer formed on shot peened specimens could sufficiently alleviate the detrimental effect caused by block exposure. However, a higher loss in fatigue strength is obtained for the eletropolished surface after block exposure. Without the deformed and hardened surface layer, the embrittlement induced by block exposure appears to have a higher degree of detrimental effect on fatigue behaviour for electropolished surface than for shot peened surface. The present results clearly indicate that with the increasingly reduced impact from surface defects, the fatigue behavior is increasingly governed by inner microstructures.

4.3. Effect of individual exposure-oxidation

Individual exposure and oxidation provides all the specimens in Group C not only the changes of bulk material but also oxidised surface layer. Both are expected to be detrimental to fatigue behaviour. However, it is surprising to find that although the fatigue performance is deteriorated when subjected to block exposure, it is markedly improved when subjected to individual exposure-oxidation. In fact, there exists a general trend in fatigue performance for almost every type of surface studied in the present work: individual exposure-oxidation (Group C) > no exposure (Group A) > block exposure (Group B).

Key explanations for the enhanced S-N fatigue behaviour in Group C are based on the fact that individual specimens have been immersed into a warm-air (700°C) environment for 10000 h after surface preparation. Firstly, the residual tensile stresses in the near surface layer introduced by the EDM process are expected to relax and dissipate significantly due to staying in such a warm environment for such a long period of time. Along with tensile stress relaxation and dissipation, surface stress raisers such as eroded holes, protruded globes and microcracks could become less sensitive to cracking. Secondly, inner stress concentration induced by phase transformations such as B2-$\omega \rightarrow \xi$ silicides and B2$\rightarrow\gamma$ due to changed atomic volume [23, 24, 42] would also be relaxed and dissipated to large degree in the warm-air environment. As a result, bulk material could become more consolidated and

integrated. Thirdly, microstructural changes occurred in the subsurface layer during individual exposure-oxidation besides precipitation of brittle particles. As observed for EDM samples of Group C, a layer of γ grains (~ 30 μm in depth) and a layer of fully lamellar colonies (~ 300 μm in depth) formed below the oxidation layer. As a consequence of the changes, brittle particles such as $D8_8$-ω and $(Ti,Nb,Zr)_5(Si,Al)_3$ silicides, and their parent phases B2+ω, are shifted to subsurface region which is about 300 μm away from the surface. Although no β(B2+ω) disappeared below the scale in shot peened and electropolished surfaces, the brittle particles inside could become less active because significant diffusion of Ti/Nb/Zr towards the surface would reduce their size and population. The stress relaxation and dissipation both at surface and in bulk material have positive effects on fatigue performance, which are contradictory to the negative effects from exposure-induced embrittlement (inner factor) and oxidation (outer factor). And the microstructural changes such as total and partial disappearance of brittle particles in the subsurface region could also reduce the probability of crack nucleation/initiation.

Consequently, the present results tell us unambiguously that the positive effects of the stress relaxation-dissipation and the microstructural changes in the subsurface layer outweigh the negative effects of oxidation layers and inducing microstructural embrittlement, resulting in enhanced fatigue behaviour after a long-term exposure. Considering the increased fatigue resistance obtained with oxidation, it is tempting to speculate that the formation of oxidised layers consisting of TiO_2 and Al_2O_3 may not be as harmful as would be expected.

The enhanced fatigue behaviour after long-term exposure-oxidation of individual specimens in this study can be tentatively called “exposure induced fatigue strengthening”. The exposure-induced fatigue strengthening behaviour was observed previously in alloy 4Nb-4Zr which was studied to assess the thermal stability of microstructure and mechanical properties by author’s group [24]. The condition is somewhat different from the present work. All the S-N fatigue specimens (10 x 10 x 70 mm^3) in that study were individually exposed for

10000 h at 700°C, followed by mechanical grinding and polishing to 1 μm finish. That means individual exposure but without oxidation. Under the individual exposure condition, testpiece run-out occurred when σ_{max} = 450MPa before exposure and when σ_{max} = 570 MPa after individual exposure at 700°C for 10000 h. It can be seen that the result before exposure (σ_{max} = 450MPa) is slightly inferior to that given by the electropolished surface in Group A (σ_{max} = 470MPa) since the surface quality is better in the present work. On the other hand, the result after exposure (σ_{max} = 570 MPa) is markedly superior to that offered by the electropolished surface in Group C (σ_{max} = 530 MPa). This 40MPa loss in individual exposure-oxidation condition, compared with the individual exposure condition, should be attributed mainly to the surface oxidation involved in the present work.

Conclusions

With the yield strength of $\sigma_{0.1}$=621MPa (641MPa after exposure), fatigue testing at present is always conducted under a loading condition of $\sigma_{max} < \sigma_{0.1}$ for the high strength alloy 4Nb-4Zr. Under this condition, plastic deformation through intense planar slipping and twining is unlikely to be activated in the surface layer where maximum stress is applied. Without intense deformation in the surface layers, the quality of the maximum-stressed surface becomes increasingly important for fatigue resistance behaviour. Based on this understanding, the fatigue befaviour of alloy 4Nb-4Zr can be well understood, and concluded as below:

1. High strength alloy 4Nb-4Zr is very sensitive to the deteriorated surface condition. Very low $\sigma_{FL}/\sigma_{0.1}$ (0.45) and σ_{FL}/σ_{UTS} (0.42) ratios are produced for EDM surface.

2. A high degree of notch sensitivity (Q=0.9) is observed for the alloy. No considerable deformation at notch root is expected, and thus no considerable “notch strengthening” can be obtained under the loading condition of $\sigma_{max} < \sigma_{0.1}$.

3. Alloy 4Nb-4Zr is also sensitive to surface improvement. Shot peening of EDM surface increases fatigue strength by 36%, while electropolishing of the surface increases by 68%

before exposure. Both the hardened surface and "defect-free" surface demand a crack nucleation phase which is difficult to occur under the loading condition of $\sigma_{max} < \sigma_{0.1}$.

4. Fatigue performances are deteriorated when subjected to block exposure. This is attributed to exposure-induced embrrittlement caused by the formation of γ grains, $D8_8$-ω particles and silicides in the β matrix. A higher loss is obtained for electropolished surface than for shot peened surface, suggesting that with the increasingly reduced impact from surface defects, the inner microstructure becomes increasingly crucial in determining fatigue performance.

5. Exposure-induced fatigue strengthening occurs on all types of surface after individual exposure-oxidation. The relaxation of residual tensile stress and dissipation of bulk stress in warm-air environment, plus decrease of brittle phases, outweigh the negative effects of oxidation layer formed and exposure-induced embrittlement. The degree of the "exposure-induced fatigue strengthening" is related reversely to the surface quality. The worst EDM surface has the greatest potential for improvement after exposure.

6. Considering the increased fatigue resistance obtained after individual exposure-oxidation, the formation of oxidised layers at the surface of alloy 4Nb-4Zr may not be as harmful as would be expected.

Acknowledgement

The authors gratefully acknowledge the National Natural Science Foundation of China for financial support (Project number: 51271154). The authors thank Mr. Hong Liang Sun for some management support during this work. The author ZWH is also very thankful to the School of Metallurgy and Materials, The University of Birmingham, U. K. for some experimental support.

References

[1]. A.W. James, P. Bowen, Mater Sci Eng A 153 (1992) 486-492.

[2]. W.O. Soboyejo, K.T. Venkateswara Rao, S.M.L. Sastry, R.O. Richie, Metall Trans A 24 (1993) 585-600.

[3]. D.L. Davidson, J.B. Campbell, Metall Trans A 24 (1993) 1555-1574.

[4]. K.T. Venkateswara Rao, Y-W. Kim, C.L. Muhlstein, R.O. Richie, Mater Sci Eng A 192/193(1995) 474-482.

[5]. Z.W. Huang, P. Bowen, in: X.R. Wu, Z.G. Wang (Eds.), Fatigue'99, 7th Intl. Fatigue Congress, HEP & Emas, Beijing, 1999, vol. III, pp. 1585-1590.

[6]. J.M. Larsen, B.D. Worth, S.J. Balsone, J.W. Jones, in: Y-W. Kim, R. Wagner, M. Yamaguchi (Eds.), Gamma Titanium Aluminides, TMS, Warrendale, PA, 1995, pp. 821-834.

[7]. R.O. Ritchie, in: X.R. Wu, Z.G. Wang (Eds.), Fatigue'99, 7th Intl. Fatigue Congress, HEP & Emas, Beijing, 1999, vol. I, pp. 3-14.

[8]. J.M. Larsen, A.H. Rosenberger, B.D. Worth, K.Z. Li, D.C. Maxwell, W.J. Porter, in Y-W. Kim, D.M. Dimiduk, M.H. Lorreto (Eds.), Gamma Titanium Aluminides, TMS Warrendale, PA, 1999, pp. 463-472.

[9]. S.J. Trail, P. Bowen, Mater Sci Eng A 192/193 (1995) 427-434.

[10]. G. Henaff, A-L Gloanec, Intermetallics 13 (2005) 543-558.

[11]. S.K. Jha, J.M. Larsen, A.H. Rosenberger, Acta Mater 53 (2005) 1293–1304.

[12]. P.E. Jones, D. Eylon, Mater Sci Eng A 263 (1999) 296–304.

[13]. A.R.C. Sharman, D.K. Aspinwall, R.C. Dewes, P. Bowen, Wear 249 (2001) 473–481.

[14]. X. Wu, D. Hu, M. Preuss, P.J. Withers, M.H. Loretto, Intermetallics 12(2004) 281–287.

[15]. J. Lindemann, C. Buque, F. Appel, Acta Mater 54 (2006) 1155–1164.

[16]. W.E. Voice, M. Henderson, E.F.J. Shelton, X. Wu, Intermetallics 13 (2005) 959–964.

[17]. M. Nazmy, M. Staubli, G. Onofrio, V. Lubinc, Scripta Mater 45 (2001) 787-792.

[18]. T.S. Harding, J.W. Jones, P.S. Steif, T.M. Pollock, Scripta Mater 40 (1999) 445–449

[19]. M.R. Bache, C.C. Morgans, Intermetallics 19 (2011) 782-786.

[20]. S.K. Planck, A.H. Rosenberger, Mater Sci Eng A 325 (2002) 270–280.

[21]. A. Zeller, F. Dettenwanger, M. Schutze, Intermetallics 10 (2002) 33–57.

[22]. H. Jiang, D. Hu, X. Wu, J Alloys and Compounds 475 (2009) 134–138.

[23]. Z.W. Huang, Acta Mater 56 (2008) 1689–1700.

[24]. Z.W. Huang, Intermetallics 42 (2013) 170-179.

[25]. H. Inui, M.H. Oh, A. Nakamura, M. Yamaguch, Acta Mater 40 (1992) 3095-3104.

[26]. R. Uemori, T. Hanamura, H. Morikawa, Scripta Metall Mater 26 (1992) 969-974.

[27]. A. Denquin, S. Naka, A. Huguet, A. Menand, Scripta Metall Mater 28 (1993) 1131-1136.

[28]. K. Hono, E. Abe, T. Kumagai, H. Harada, Scripta Mater 1996;35:495-499.

[29]. A. Menand, A. Huguet, A.Nerac-Partaix, Acta Mater 44 (1996) 4729-4737.

[30]. M. Yoshihara, K. Miura, Intermetallics, 3 (1995) 357-363

[31]. Y. Shida, H. Anada, Corrosion Science 35 (1993) 945-953.

[32]. D.B. Lee, S.W. Woo, Intermetallics 13 (2005) 169–177.

[33]. J.P. Lin, L.L. Zhao, G.Y. Li, L.Q. Zhang, X.P. Song, F. Ye, G.L. Chen, Intermetallics 19 (2011) 131-136.

[34]. N. Zheng, W.J. Quadakkers, A. Gil, H. Nickel, Oxidation of Metals 44 (1995) 477-499.

[35]. I.E. Locci1y, M.P. Brady, R.A. MacKay, J.W. Smith, Scripta Mater 37 (1997) 761-766.

[36]. Pe´rez P, Jime´nez JA. Frommeyer G, P. Adeva, Mater Sci Eng A 284(2000)138–147.

[37]. S.L. Draper, D. Isheim, Intermetallics 22 (2012) 77-83.

[38]. T.S. Harding, J.W. Jones, Scripta Mater 43 (2000) 623–629.

[39]. Z.W. Huang, S. Huang, unpublished results, 2014.

[40]. Acta Mater 47 (1999) 3189–3203.

[41]. Z.W. Huang, P. Bowen, I.P. Jones, Philosophical Mag A 81 (2001) 2183–2197.

[42]. D. Zhang, G. Dehm, H. Clemens, Scripta Mater 42 (2000) 1065-1070.

Table 1 The preparation procedure of the maximum stressed surface for fatigue tests

Surface	Preparation procedure
EDM wire	One pass EDM wire to shape
V notch (Kt = 3)	One pass EDM wire to shape
Shot peening	One pass EDM to shape, grinding, shot peening
Electropolishing	One pass EDM to shape, grinding and polishing, electropolishing

Table 2 Surface roughness Ra (μm) with error range for each surface condition

Specimen (Group)	EDM (A, C)	Shot peening (A, C)	Electropolishing (A, C)	EDM (B)	Shot peening (B)	Electropolishing (B)
Surface roughness Ra (μm)	4.60±0.13	1.51±0.20	0.31±0.03	5.22±0.10	1.55±0.11	0.32±0.04

Table 3 S-N fatigue results and data analysis for EDM, shot peening and electropolishing specimens ($\sigma_{0.1}$=621MPa before exposure, $\sigma_{0.1}$=641 MPa after exposure)

Exposure Condition (Group)	Specimen surface Condition	σ_{FL} (MPa)	$\sigma_{FL}/\sigma_{0.1}$	Increase in σ_{FL} (%) relative to EDM	Change in σ_{FL} (%) relative to Group A
No exposure (Group A)	EDM wire	280	0.45	—	—
	Shot peening	380	0.61		
	Electronpolishing	470	0.76	36	
Block exposure (Group B)	EDM wire	240	0.37	—	-14
	Shot peening	350	0.55		-8
	Electronpolishing	340	0.53	46	-28
Individual exposure -oxidation (Group C)	EDM wire	450	0.70	—	61
	Shot peening	475	0.74		25
	Electronpolishing	530	0.83	6	13

Table 4 S-N fatigue results and data analysis for V notch (K_t=3) specimens ($\sigma_{0.1}$=621MPa)

Exposure condition (Group)	σ_{FL} (MPa)	$\sigma_{FL}/\sigma_{0.1}$	K_f	K_f/K_t	Notch sensitivity factor Q
No exposure (Group A)	100	0.16	2.80	0.93	0.90
Block exposure (Group B)	120	0.19	2.00	0.67	0.50
Individual exposure-oxidation (Group C)	170	0.27	2.65	0.88	0.83

Captions

Fig. 1 (a, b) SEM BSE and (c, d) TEM BF images showing the microstructure of alloy Ti-44Al-4Nb-4Zr-0.2Si-1B (a, c) before and (b, d) after exposure at 700°C for 10000 h

Fig. 2 SEM images showing (a) the normal and (b) cross sectional view of the EDM surface before exposure

Fig. 3 (a) The normal (SE) and (b-d) cross sectional view (BSE) of the shot peened surface before exposure. (c) Barely deformed surface due to a hard orientation of lamellae. Dynamic recrystallisantion (DR) occurred inside (c) a lamellar colony and (d) an equiaxed γ grain

Fig. 4 Micro hardness profiles of shot peened specimens before and after thermal exposure

Fig. 5 (a) BSE image showing the electropolished surface before exposure, (b) an SE image showing the smooth surface (arrowed) after electropolishing.

Fig. 6 (a) The normal view (SE image), and (b), (c) cross sectional view (BSE images) of the EDM surface after individual exposure-oxidation at 700°C for 10000 h. Note that the oxidation layer is ~ 25 μm thick, followed by a γ-grain layer (~ 30 μm thick), and the β-free zone is about 300 μm deep.

Fig. 7 (a) The normal view (SE), and (b), (c) cross sectional view (BSE) of the shot peened surface after exposure-oxidation at 700°C for 10000 h. Note that the oxidation scale is ~ 15 μm thick, followed by a subsurface region (~ 35 μm thick) covered by a high density of white particles.

Fig. 8 (a) The normal view (SE) and (b) cross sectional view (BSE) of the electropolished surface after exposure-oxidation at 700°C for 10000 h. Note that the oxidation scale is ~ 10 μm thick, followed by a subsurface region (~ 50 μm thick) covered by a high density of white particles

Fig. 9 S-N fatigue performance of four types of surface in three exposure groups: (a) Group A (no exposure), (b) Group B (block exposure without oxidation), (c) Group C (individual exposure and oxidation).

Fig. 10 S-N fatigue performance of four types of surface in three exposure conditions: (a) EDM, (b) shot peening, (c) electropolishing and (d) V notch (A, B, C denote Group A, B, and C, respectively).

Fig. 11 SEM images showing (a) the fracture surfaces after fatigue at σ_{max}= 600 MPa and N_f = 2300 cycles (electropolished surface before exposure).

Figure1

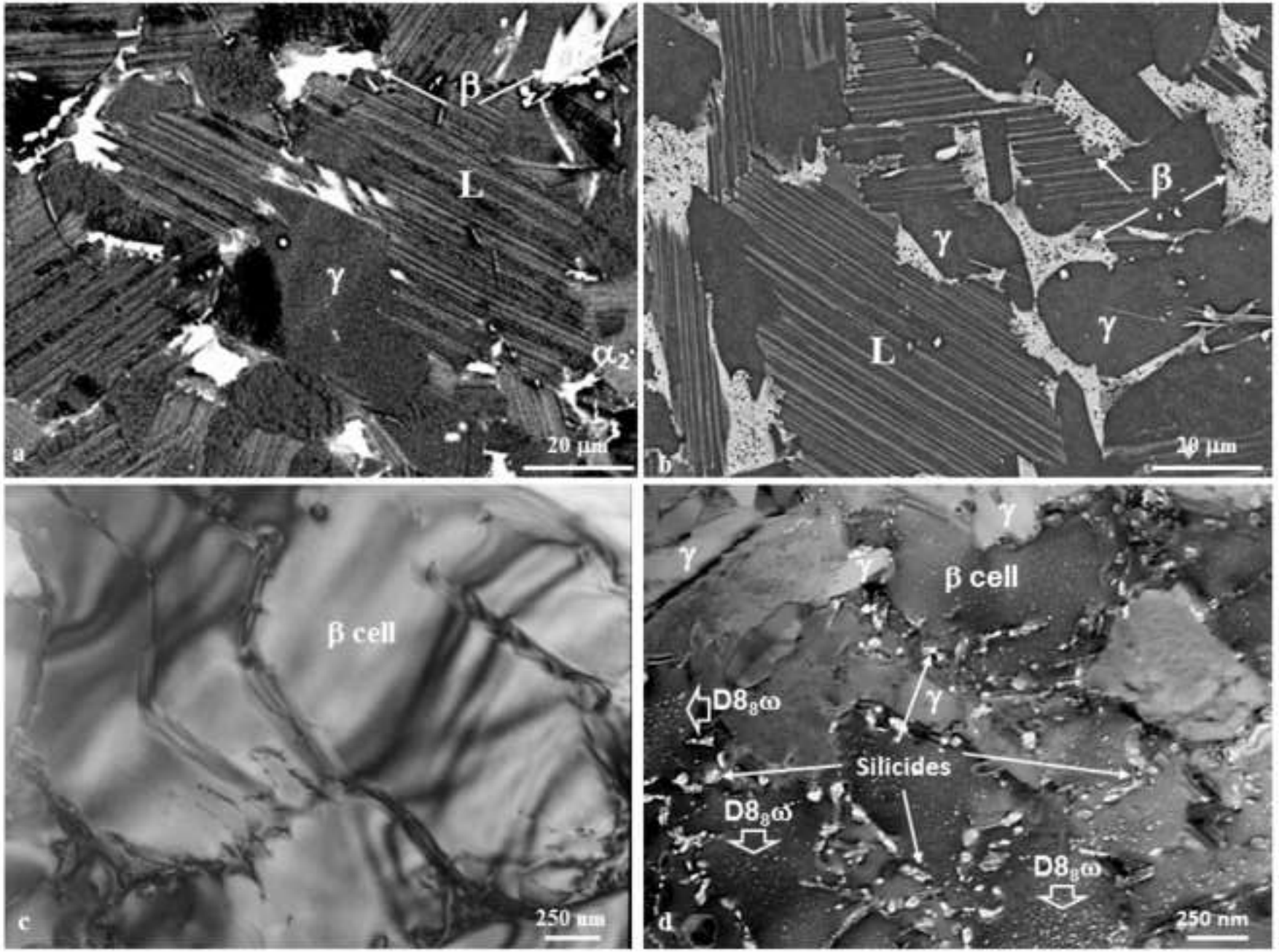

Fig. 1 (a, b) SEM BSE and (c, d) TEM BF images showing the microstructure of alloy Ti-44Al-4Nb-4Zr-0.2Si-1B (a, c) before and (b, d) after exposure at 700°C for 10000 h.

Figure2

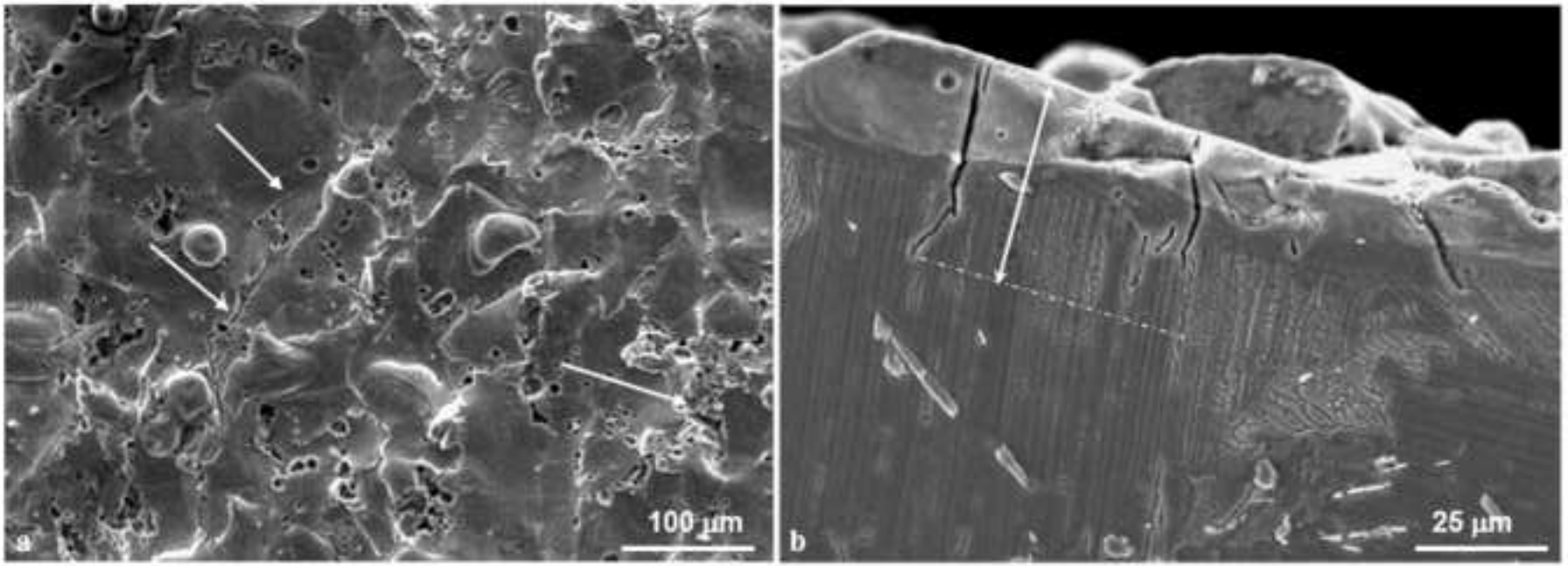

Fig. 2 SEM images showing (a) the normal and (b) cross sectional view of the EDM surface before exposure.

Figure3

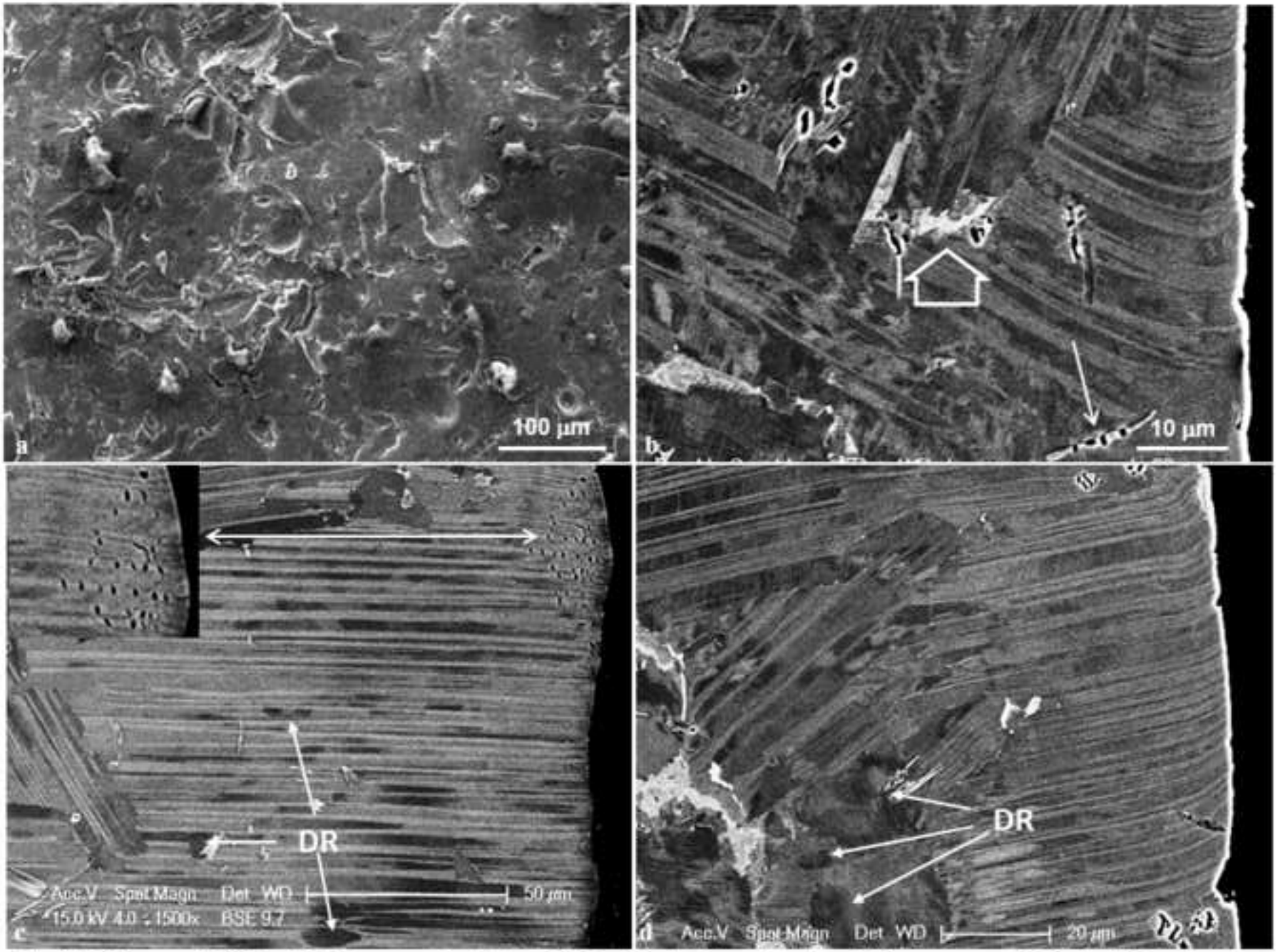

Fig. 3 (a) The normal (SE) and (b-d) cross sectional view (BSE) of the shot peened surface before exposure. (c) Barely deformed surface due to a hard orientation of lamellae. Dynamic recrystallisantion (DR) occurred inside (c) a lamellar colony and (d) an equiaxed γ grain.

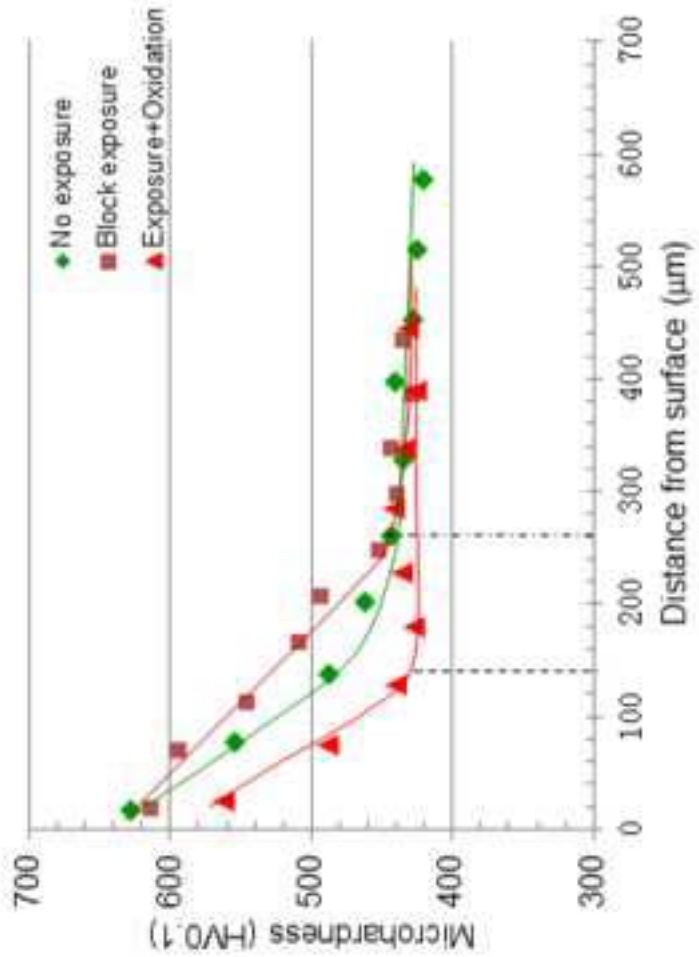

Fig. 4 Micro hardness profiles of shot peened specimens before and after thermal exposure.

Figure4

Figure5

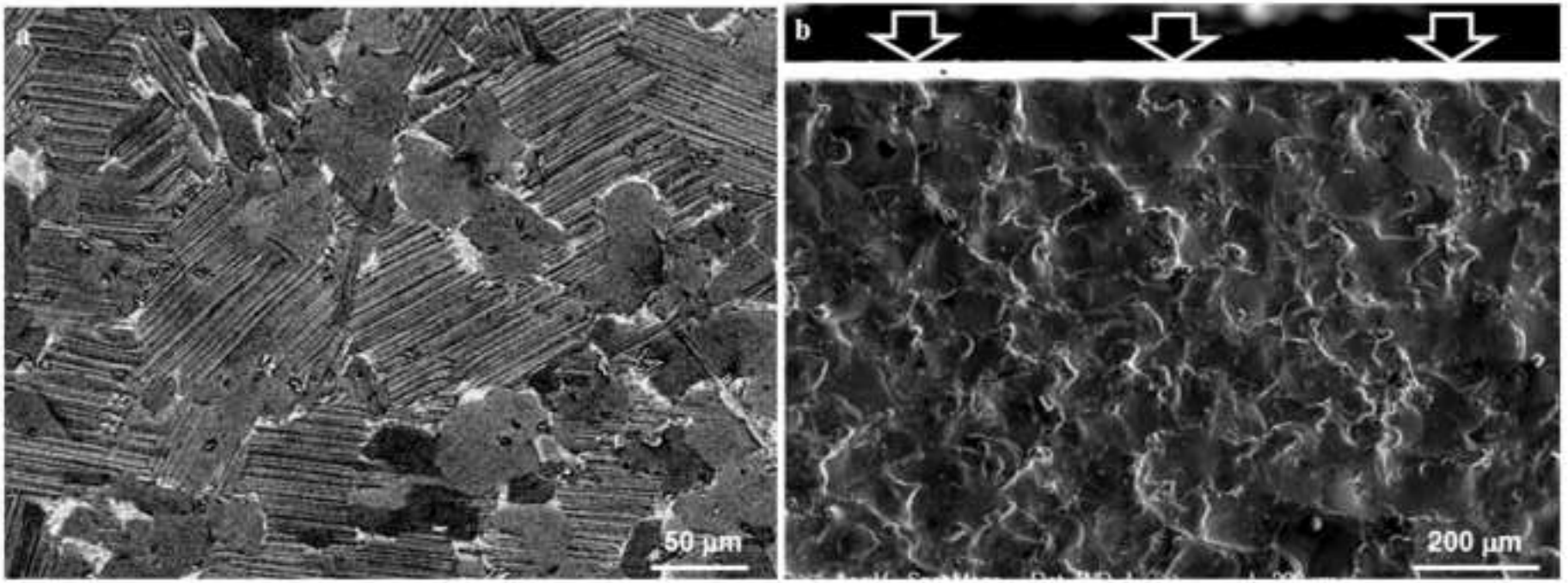

Fig. 5 (a) BSE image showing the electropolished surface before exposure, (b) an SE image showing the smooth surface (arrowed) after electropolishing.

Figure6

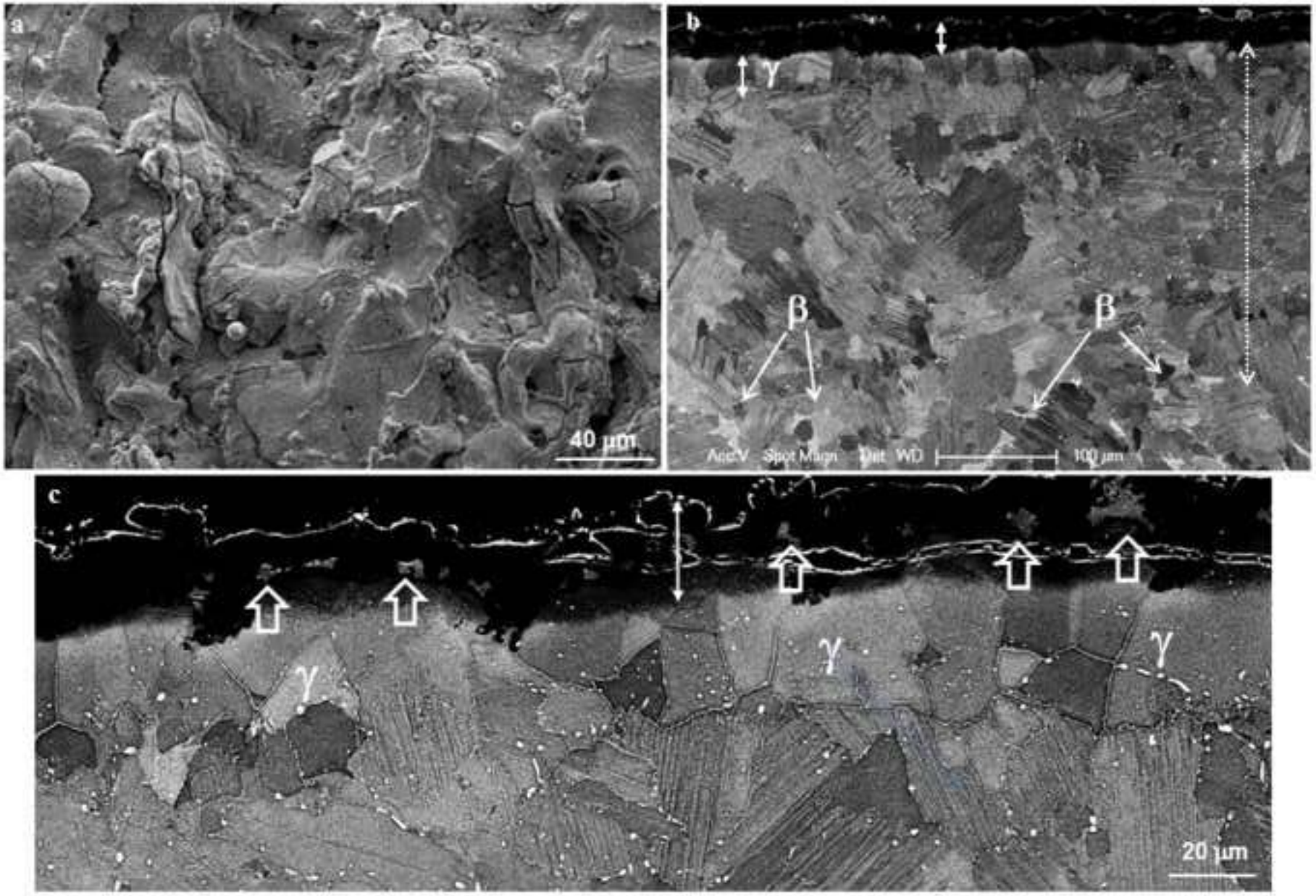

Fig. 6 (a) The normal view (SE image), and (b), (c) cross sectional view (BSE images) of the EDM surface after individual exposure-oxidation at 700°C for 10000 h. Note that the oxidation scale is ~ 25 μm thick, followed by a γ-grain layer (~ 30 μm thick), and the β-free zone is about 300 μm deep.

Figure7

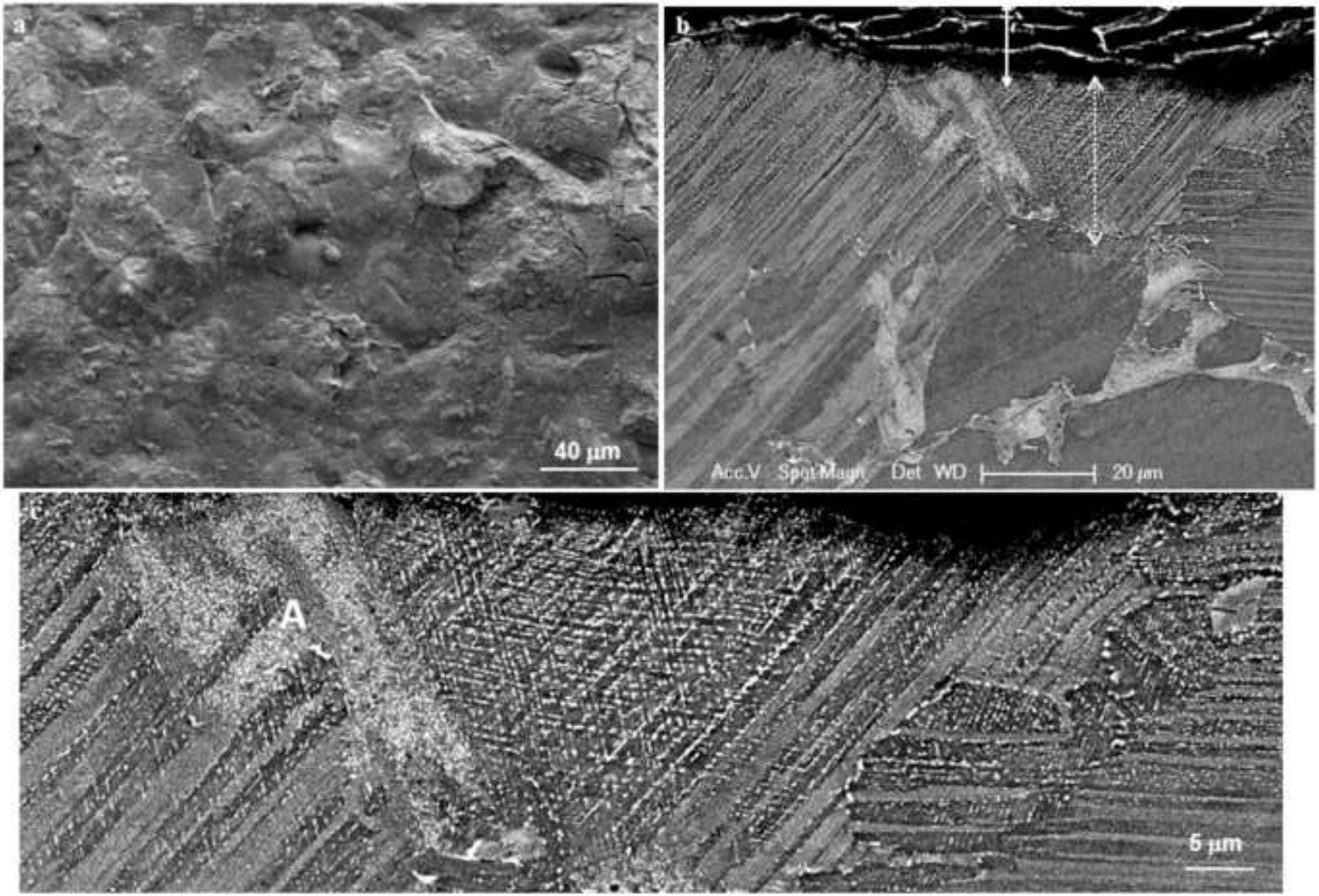

Fig. 7 (a) The normal view (SE), and (b), (c) cross sectional view (BSE) of the shot peened surface after exposure-oxidation at 700°C for 10000 h. Note that the oxidation scale is ~ 15 μm thick, followed by a subsurface region (~ 35 μm thick) covered by a high density of white particles.

Figure8

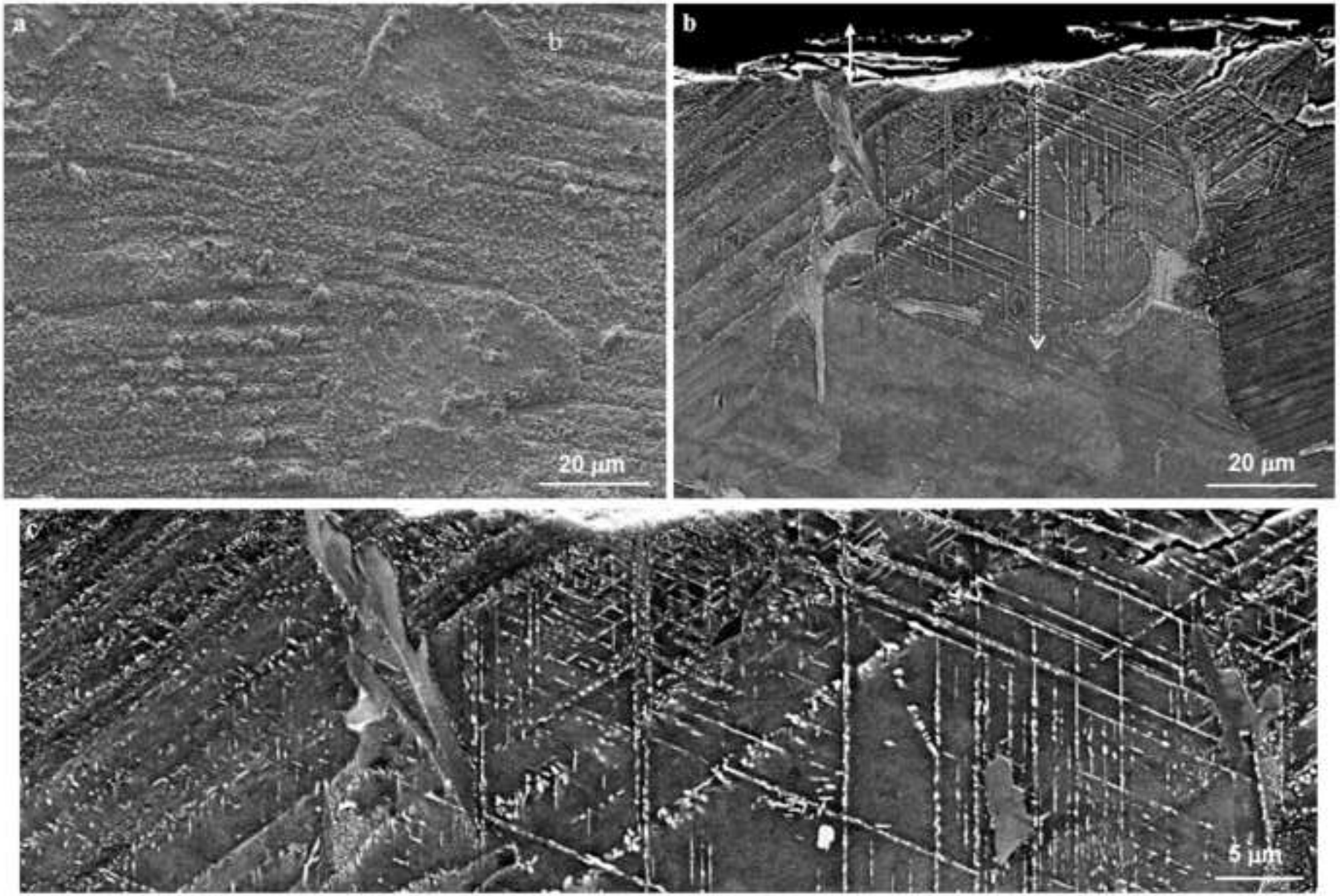

Fig. 8 (a) The normal view (SE) and (b) cross sectional view (BSE) of the electropolished surface after exposure-oxidation at 700°C for 10000 h. Note that the oxidation scale is ~ 10 µm thick, followed by a subsurface region (~ 50 µm thick) covered by a high density of white particles.

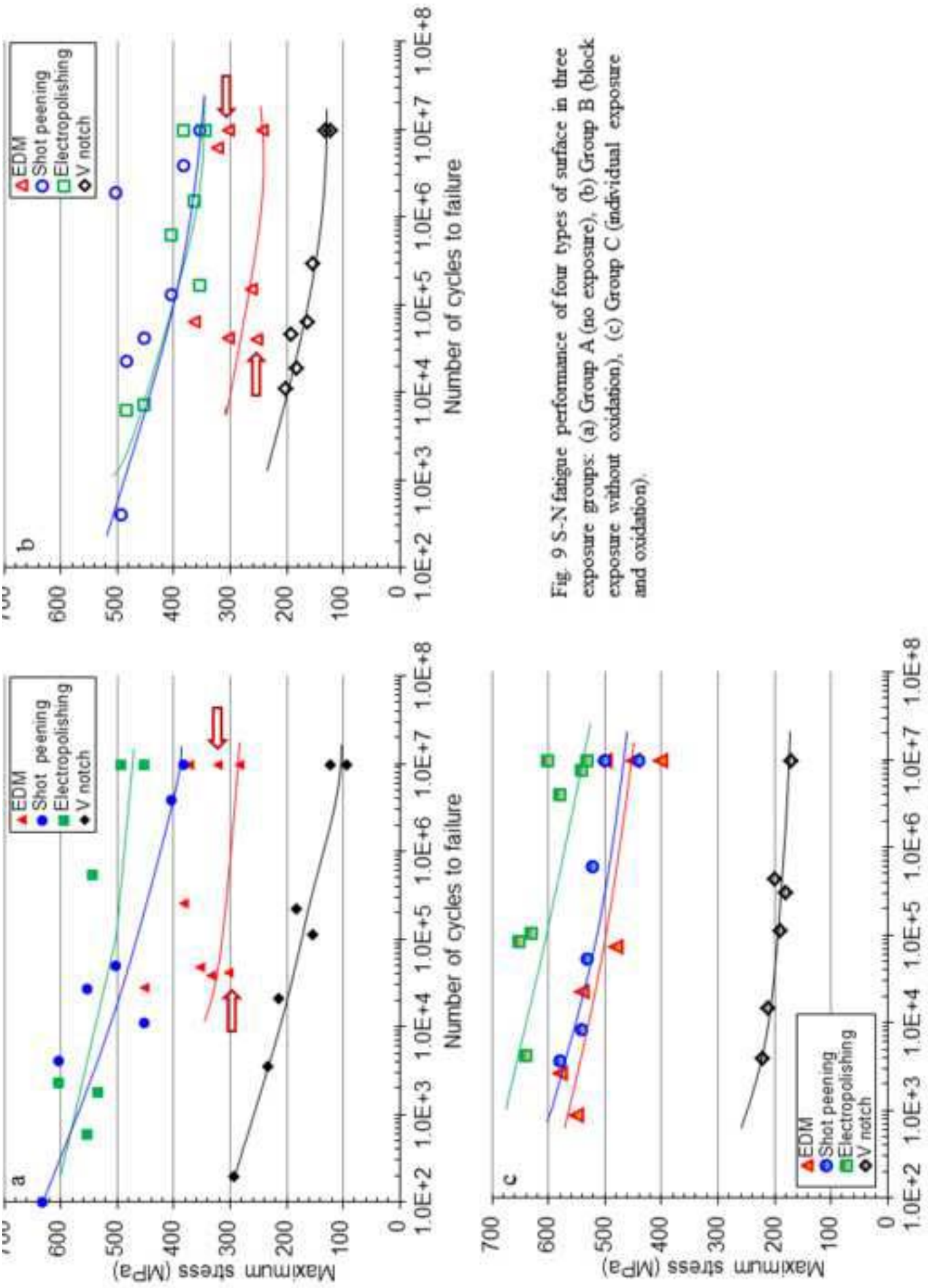

Fig. 9 S-N fatigue performance of four types of surface in three exposure groups: (a) Group A (no exposure), (b) Group B (block exposure without oxidation), (c) Group C (individual exposure and oxidation).

Figure9

Figure10

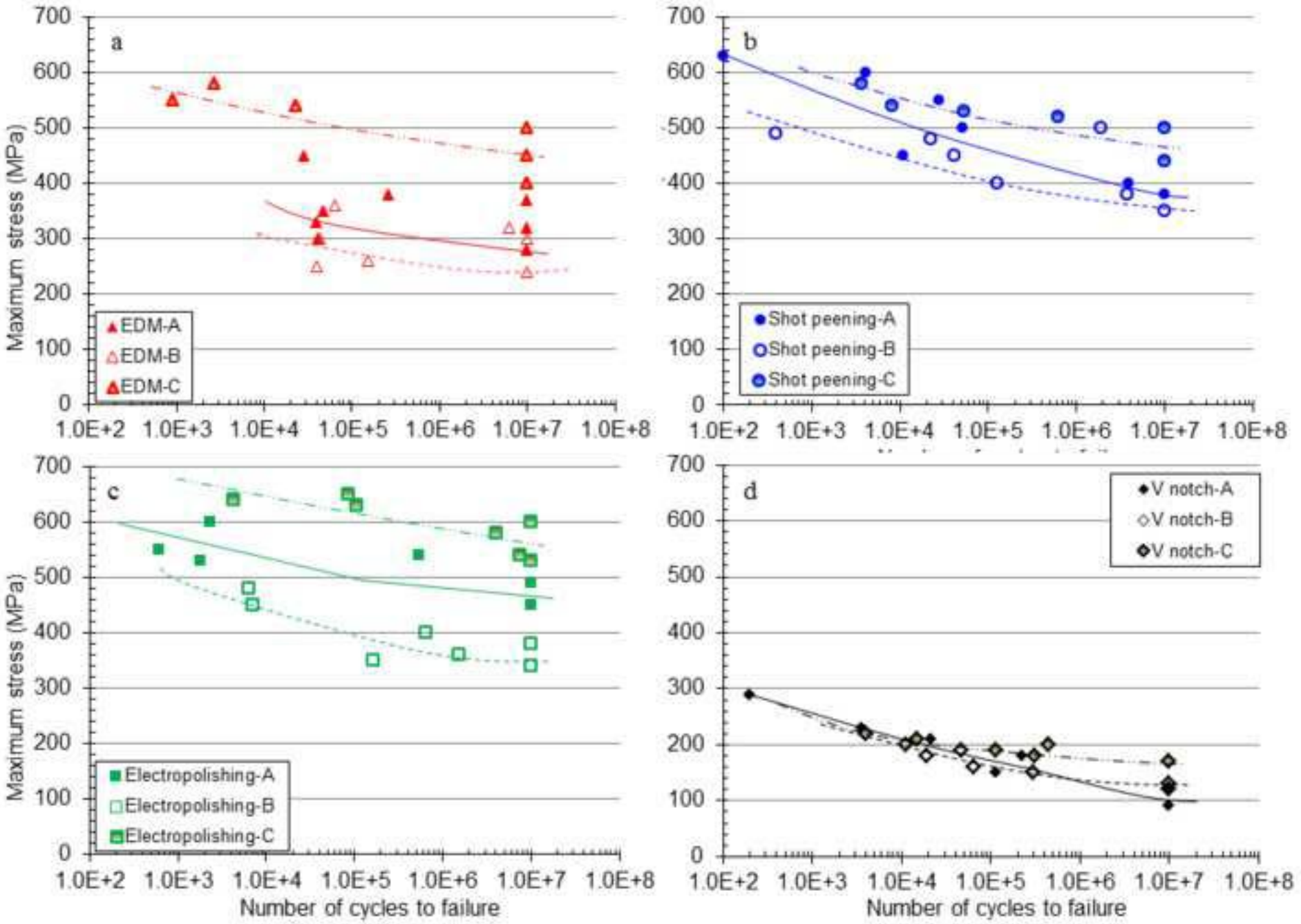

Fig. 10 S-N fatigue performance of four types of surface in three exposure conditions: (a) EDM, (b) shot peening, (c) electropolishing and (d) V notch (A, B, C denote Group A, B, and C, respectively).

Figure11

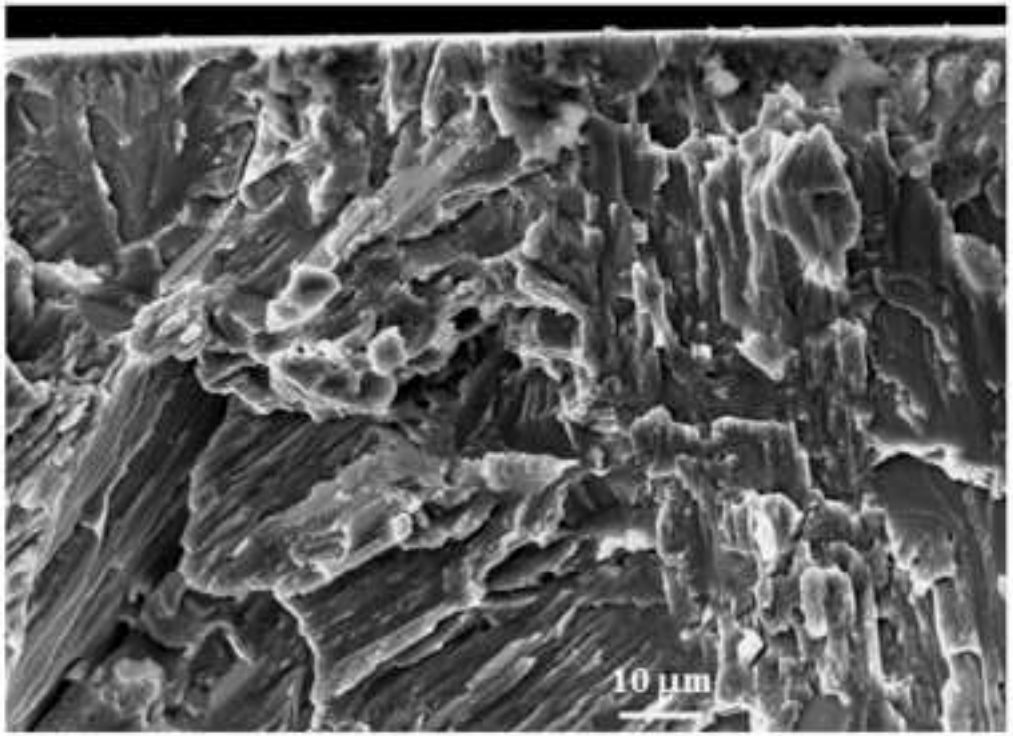

Fig. 11 SEM images showing (a) the fracture surfaces after fatigue at σ_{max}= 600 MPa and N_f= 2300 cycles (electropolished surface before exposure).